Edge Hill University

The Department of Computer Science

Finding the density of tumor cells from Histopathological images

CIS3161 CW2 – Project report

Student: Mohammed Rahman Sherif

Supervisor: Ardhendu Behera

Date: 10-05-2022

This Report is submitted in partial fulfilment of the requirements for the BSc Honours Computing (or Web Systems Development, or Computer Science) Degree at Edge Hill University

Abstract:

Computer-assisted breast cancer detection is a useful and widely used technique that aids pathologists in making clinical diagnoses and running their businesses more efficiently. In existing research, breast cancer identification is based mostly on a single imaging characteristic. We propose the use of Resnet 50, which is a state-of-the-art technique, for these types of detecting issues. To begin, we extract a complementary characteristic known as cell group, which is used to compute the density of tumour cells, one of the cell group's categories. For training and evaluating our Resnet50 model, we try to divide all of the pictures in the NuCLS dataset into two groups. The data pre-processing and augmentation are carried out in accordance with standard processing protocols, which we will go over in detail below. We use various combinations of learning rates, trainable layers, optimizers, and other elements to create and construct our models' multiple times. Finally, we compare the results of all the models and iterations. Our analyses reveal that the Resnet 50 model, which has all layers trainable using the learning rate obtained by performing hyperparameter tuning, outperforms baselines on normalised histopathological validation picture data. Our method encourages the use of hyperparameter adjustment to combat overfitting.

Table of Contents

List of Figures:

List of Tables

Chapter 1: Introduction

1.1. Introduction:

In 2020, breast cancer is the most common disease which affected over 2.26 million people which tremendously surpasses lung cancer and as per American Cancer Society report, 1 in 8 women is getting affected by breast cancer in their lifetime. This latest data has been revealed by International Agency for Research on Cancer under WHO. This disease drastically endangers the life and health of women. Cells, tissues, or gland of the breast are vulnerable for breast cancer. The breast tumour is commonly known as two types: benign and malignant. Positive bags are generated from malignant images whereas negative bags are generated from benign images (Figure 1). The use of modern whole-slide digital scanners to digitise histological specimens provides not only the benefit of easy image storage, visualisation, and analysis, but also the ability to apply automatic image analysis techniques to digital histological slides to provide accurate quantifications (e.g., tumour extent and nuclei counts) and classifications of tumour sub-types, with the goal of reducing both inter- and intra-reader variability. The benign tumour is not cancerous and it's not a highly risky factor whereas the malignant is highly risky which is the primary cause of breast cancer. For detection of breast cancer, pathological diagnosis is widely used which intern has a benchmark in cancer detection. histopathological images are primarily used for pathological diagnosis. Nowadays, deep learning is achieving excellent result in various computer vision tasks, such as image classification (Hongbin., 2020), regression, object detection (Zhongqiu, 2019), and image segmentation (Guotai, 2017). To be more specific, Convolutional neural networks has an ability in analysing and learning patterns from the image data.

What is Resnet and the need for it?

A series of developments in the field of computer vision have occurred in recent years. By receiving state-of-the-art results on challenges like picture classification and image recognition, especially since the introduction of deep Convolutional neural networks. As a result, researchers have tended to build deeper neural networks (with more layers) to perform such complex tasks and improve classification/recognition accuracy over time. However, when we add more layers to the neural network, it gets more difficult to train them, and their accuracy begins to saturate and ultimately decline. ResNet comes to the rescue and assists in the resolution of this issue.

We usually stack some additional layers in Deep Neural Networks to address a complex problem, which improves accuracy and performance. The idea behind adding more layers is that they will learn increasingly complicated features over time. In the case of picture recognition, the first layer might learn to recognise edges, the second layer might learn to identify textures, and the third layer might learn to recognise objects, and so on. However, it has been discovered that the classic Convolutional neural network model has a maximum depth threshold.

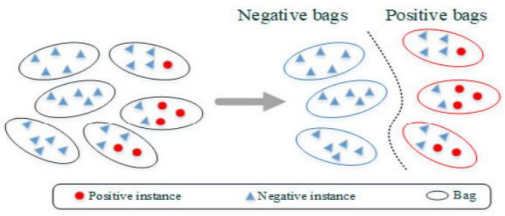

Figure 1.1: Schematic diagram of MIL

1.2. Aim:

The aim of this project is to find the density of tumour cells using histopathological image data for detecting Breast Cancer via pre-trained Deep Neural Network model.

1.3. Objective:

- Find the density of tumour cells from the histopathological image dataset

by dividing the total number of tumour cell present in a single image divided by the total number of other cells present in the same image except tumour.

- It is essential to feed a greater number of images for getting higher accuracy while predicting. so, data augmentation is required with Random Rotation, Random Flip, Random Translation, and Random Contrast to enhance the performance of the AI model and to prevent the model from overfitting and underfitting.
- Its mandatory to pre-process the data before inputting the image data to the network. This is because of the variation in the shape, size, dimension, colour mode, label, of the images and to prepare the data for some other additional functions like splitting and validating.
- Want to train a model using pre-trained weights and architecture of different model such as Resnet 50 (Kaiming, 2015), Resnet 101 (Kaiming, 2015), Resnet 152 (Kaiming , 2015) and each model with different layer optimizations.
- Ensure that the model performs well with the test data and validation data where the expected range of MSE should be decreased as much as possible and need to be evaluated with appropriate metrics and visualizations.

1.4. Ethics:

The requirement of Artificial Intelligence systems has a substantial amount of high-quality data for training, testing, and validation, data ownership, as well as data security, are critical concerns (Nadia, 2019). The increasing entry of huge technology businesses like Google and IBM into medical field, as well as the profusion of new companies producing breast cancer-based inventions (Fenech, 2018), make this more difficult. Some governments and research agency made medical data available to engineers: for an instance, the Italian legal representatives gave IBM Watson exclusive usage rights to all sixty-one million Italians' anonymized health records, including genome data, without obtaining specific consent from individuals. Such disclosures raise serious questions about what public values must be exchanged for the transfer of these extremely rich datasets to MNC companies (Leshem, 2019). As evidenced by several cyber-crime operations, like the 2016 Australia event Medicare Benefits Schedule Re-identification, expanding data utilisation also rises potential for data leak and re-identification. Google used data from the University of Chicago Medical Centre to construct a predictive Artificial Intelligence powered EHR atmosphere; by the writing time, Google and IBM are prosecuted by law and affairs for professed exploitation of patient electronic health record data. The case is based on Google's capacity to re-identify electronic health-data by tying it to their massive geolocated and individuated datasets. At this size and in such a dynamic context, traditional opt-in or opt-out consent methods are highly challenging to execute. Patients those who did not provide their medical are unable to obtain gold-standard therapy if AI algorithms require specific individual healthcare and physicians depend on this algorithm for taking decisions, forming an anger between quality of care and consent (Azencott, 2018).

If the truth of clinical care AI is to be flown in a reasonable and appropriate fashion, these data-related challenges must be addressed. Some Artificial Intelligence engineers are exploring with novel data security methods. Participants in the DREAM Challenge, for example, are not allowed access to data and instead had to send their script to the DREAM server using a Docker container, which is a self-container folder of software package that will be shared and run in-between systems.

The Docker had access to DREAM data when it was run on the DREAM server, allowing every neural architecture to need to be to be trained and assessed on the same image data (Stacy, 2020). The rivals got their findings, but not the image or health care information. For any clinical system interested in implementing deep learning (DL) applications, struggle with the data preservation addition with utilisation in such a granular way will be a vital primary step (Guangli, 2021).

Chapter 2: Project background and literature review

2.1. Project background:

The procedure preserves the underlying tissue architecture, histopathology images provide clear and thorough perspective of disorders and its effectiveness on tissues. As a result, some disease characteristics, such as lymphocytic infiltration of cancer, may only be determined by looking at a histopathological scan. Diagnosis from a histopathological image is still "gold standard" for diagnosing wide range of illnesses, adding practically all kinds of cancer. While the extra structure in pathological image provides a range of information, it additionally introduces a new batch of obstacles for automated image interpretation. From a diagnostic standpoint, it is believed that correct use of this spatial info will permit for more particular characterizations of picture. The approaches used to assess cytology imaging have typically been applied to histopathology imagery analysis. Certain features of nuclei are indicators of malignant situations. Thus, quantitative measurements for malignant nuclei were devised and evaluated on cytology imagery to suitably include the general observations of an expert pathologist. If histology structures like cell nuclei, glands, and lymphocytes have been properly segmented, these same metrics can be utilised to analyse histopathology images. Moreover, almost every automated histopathology picture analysis algorithm now uses spatial analysis of histopathology data as their backbone. Despite the advances made thus far, because of the range of imaging modalities and disorder-specific characteristics, this is still a vast area of open research.

2.2 Literature review:

Breast cancer is one of the deadliest diseases in the world which has reached over 2.26 million cases in 2020. It tremendously harms women’s health and life. Breast cancer's history is a tangled web of attempts to comprehend the elusive nature of this hormone-responsive malignancy and physicians' determination to defeat it through physical removal (surgery), cell annihilation (chemo-radiotherapy), or targeted therapy to cell receptors (biomodulation) (Ritu, 2014). Since the location of the organ allowed for easy identification, written accounts, and pictures of breast cancer date back to antiquity. The Edwin smith surgical papyrus, which dates from 3,000–2,500 B.C. and is thought to have been written by Imhotep (an Egyptian physician-architect), contains accurate tales of breast cancer. If the cancer was "cold to the touch, bulging, and spread all over the breast," the condition was considered incurable. As demonstrated by votive offerings in the shape of breasts in Greek temples that housed Asclepius, the god of medicine, a divinity was exhorted to grant cure from breast diseases in ancient Greece. In the medical language, the terms carcinoma (carcinoma), scirrhous (hard, Greek Skyros), and cacoethes (malignant disease, Greek cacoethes) all derive from Hellenistic texts. Hippocrates' notion of humour imbalance as a cause of disease (about 400 B.C.) and his classic descriptions of the progressive stages of breast cancer, represent early hypotheses on the cause of cancer. In the first century A.D., Leonidas of Alexandria, following Greek traditions, courageously and deftly outlined his approach of incision and cautery. His requirement that a large margin of excision be left and that only small tumours be removed foreshadows the biomedical principles of modern surgical treatment. Galen determined that breast cancer in A.D. 200 was a systemic

disease after attributing it to the formation of black bile in the blood. The end of menstruation, according to these ancient physicians, was somehow known to cause cancer; in actuality, it was most likely due to the association of cancer with old age. Galen permitted surgical injuries to flow freely to get rid of the black bile and frowned on the use of ligatures in accordance with this notion. He invented the term "crab" for cancer to describe the dilated veins emanating from the tumour.

On the other hand, as per the data suggests, a cross-sectional analysis for 546 women has been conducted to find relationships between breast size and tumour density, status of lymph nodes, invasion of vascular or lymphatic, p53, histologic, and nuclear grade, tumour differentiation, index of mitotic, tumour necrosis, bcl-2, proliferation of ki-67, oestrogen, and c-erb-b2. For the cancer-free breast, breast size was classified as fatty or dense. All tumour markers were assessed by a single pathologist. It has been analysed whether interval cancer or cancer discovered on a screen influenced the connections (Erin, 2005). Women with tumours greater than 1.0 cm were more likely than women with tumours smaller than 1.0 cm to have thick breasts. In screen-detected malignancies, breast size was connected to tumour density, status of lymph node, and invasion of vascular or lymphatic. In lady detected with interval cancer, breast density was inversely related to histologic grade and mitotic index. However, these findings suggest that breast size relates to tumour density, lymph node status, along with lymphatic / vascular invasion in screen-diagnosed cancer. Similarly, the connections between subsequent breast cancer and breast density based on tumour traits have generated unclear results, according to a few additional research. The study added 1042 postmenopausal ladies who had been detected with breast cancer (Lusine, 2011). According to the findings, maximum mammographic density is connected to highly aggressive tumour characteristics as well as in situ malignancies.

Following a healthy lifestyle, which includes weight control and a high-quality diet, has an impact on both the risk of getting BC and the outcomes after diagnosis. Obesity is mostly caused by a sedentary lifestyle and bad eating habits, which include an excessive intake of high-calorie meals (high in sugar and saturated fats) and a low intake of nutritious foods (high in omega-3 fatty acids, natural antioxidants, and fibre). Increased adipose tissue inflammation results from this syndrome, creating a favourable milieu for BC growth and progression. Microenvironment does, in fact, have a lot of evidence (Paola, 2019). Obesity is linked to a higher incidence of postmenopausal BC, as well as BC recurrence and mortality. A systematic literature review and meta-analysis of 82 follow-up studies found a link between BMI and BC survival, with 213,075 BC survivors and 41,477 deaths (23,182 deaths attributed to BC). For each 5 kg/m2 BMI increment I before BC diagnosis, (ii) less than 12 months after diagnosis, and (iii) 12 or more months after diagnosis, respectively, an increased risk of 17 percent, 11 percent, and 8% for overall mortality and 18 percent, 14 percent, and 29% for BC-specific mortality has been observed (Chan, 2012). In addition to BMI, some studies have found a substantial link between waist-hip ratio and BC mortality in postmenopausal women (George, 2016).

Several nutrition intervention trials in BC patients have been done to improve health outcomes during chemotherapy. The Women's Intervention Nutrition Study (WINS) and the WHEL study were the two larger studies. The first involved 2437 postmenopausal women with stage I or II breast cancer who were getting standard cancer treatment. The idea that reducing dietary fat improves relapse-free survival rate was explored in this study. Fat intake was lowered from 29.2 percent to 20.3 percent of total calories in the intervention group,

although nutritional adequacy was maintained. Relapse-free survival in the intervention group was 24 percent greater than in the control group after a median follow-up of 5 years (30 percent of total energy from fat). Furthermore, women with ER or/and PR disease had a higher relapse-free survival rate than women with receptor-positive disease. Furthermore, a significant weight loss of roughly 6 pounds has been noticed. Reducing fat (fats, oils, and sweets) did not, however, imply that people made healthier choices; in fact, the percentage of people who ate fruit and vegetables increased. Thus, changes in the intervention group's intake of other nutrients besides lipids may have influenced the chance of BC recurrence (Chlebowski, 2006). The WHEL research, which looked at a different nutritional intervention in 3080 pre- and postmenopausal individuals with early-stage illness, was the second randomised controlled trial. Increased vegetable servings (five servings/day and 16 oz of vegetable juice), fruit (three servings/day), and fibre (30 g/day) intake, and reduced fat intake (15–20 percent of total calories) were part of the dietary intervention. BC survivors were given telephone counselling and culinary sessions to help them stick to their post-diagnosis diet. Furthermore, the control group was advised to consume at least five servings of fruits and vegetables every day (five-a-day advice). There is no indication that adopting a dietary pattern high in vegetables, fruit, and fibre and low in fat protects BC recurrence or death after a 7.3-year follow-up period (Pierce, 2007). A recent prospective trial, the Cancer Prevention Study-II Nutrition Cohort (CPS-II Nutrition Cohort), looked at whether pre- or post-diagnostic food intake that followed the American Cancer Society's (ACS) cancer prevention recommendations was linked to BC mortality in 4452 BC survivors. While there was no link discovered between fruit and vegetable eating and BC survival, there was a link between red and processed meat consumption and overall mortality (McCullough, 2016). The association between post-diagnosis dairy intake and increased overall mortality among women diagnosed with early-stage invasive BC was investigated in the Life After Cancer Epidemiology (LACE) study. In the first analysis, there was no statistically significant relationship; however, in a second sub-analysis, high-fat dairy consumption was linked to overall and BC-specific mortality. These findings backed with the theory that dairy fat consumption raises oestrogen levels (Kroenke, 2013).

Dietary fibre consumption in BC survivors and its association to prognosis has recently been studied. Fibre intake of >8.8 g/day was found to be negatively linked with BC-specific and overall mortality in the Health, Eating, Activity, and Lifestyle (HEAL) trial (n = 1183 survivors) (Belle, 2011). A separate cohort study (n = 516 survivors) found an inverse relationship between dietary fibre intake and overall mortality, which is consistent with these findings (McEligot, 2011). Only cereal fibres were linked to a lower risk of overall mortality after initial BC diagnosis in the Nurses' Health Study (n = 3846), whereas the WHEL trial found no link between high fibre consumption and BC events or mortality (Pierce, 2007). Overall, data suggests that dietary fibre intake (at least 10 g/day, about equivalent to three slices of whole grain bread) reduces all-cause mortality risk by about 12% (Kwan, 2009).

Chapter 3: Methodology

The problem will be approached with the use of Deep Neural Networks. A group of algorithms that attempts to recognise underlying relationships in a batch of data using a method that mimics how the human brain works is called as neural networks. Neural networks, in this context, refer to a collection of neurons that can be organic or artificial in nature. As per our concept, firstly, a bunch of images will be collected along with the ground truth which is known as dataset. Here, the ground truth consists of feature and

label information of the images. The descriptive properties of the image are the features, and the label is what is expected to predict or forecast. The images and its corresponding ground truth will be pre-processed and augmented with the standard pre-processing technique (Afshine, 2018). The data is altered in data augmentation to create more photos or images that will construct a solid learning model and the act of changing an input dataset to make it more suited for training and testing is known as data preparation or data pre-processing. Then it will be transmitted to a pre-trained model for training. A pre-trained model is one that has already been taught to address a similar problem. Instead of beginning from scratch to address a similar problem, a model trained on another problem might be used (For instance Resnet50, Resnet101 or Resnet 152). The training of the tumour density prediction model will take place with the same weights and architecture of the pre-trained model. The approach which is followed is a state-of-an-art technique for getting accurate prediction. Here, instead of making a single model, multiple models will be created with different pre-trained models and not only models, but it is also expected to create multiple models by changing parameters like learning rate from 1e-1 to 1e-6 in each and every pre-trained model. The learning rate is a parameter that governs how much the model changes every moment the model weights are changed in accordance with the predicted error. Subsequently, every model will be computed and compared with different metrics like training loss, validation loss, Mean Absolute Error (MAE), Mean Squared Error (MSE), Mean Squared Logarithmic Error (MSLE), and Root Mean Squared Error (RMSE). Finally, the model with least validation loss will be selected for prediction of tumour density.

3.1 Finding Tumour Density:

It's essential to make the NuCLS dataset ready for the implementation and to read the .csv files found in the folder contours. Using python library called pandas (NumFOCUS, 2008), it is possible to read the .csv (comma separated files). it is mandatory to read the .csv files information because it consists of the cell information of every image. There are 1440 image in total and the total number of images are same as the total number of .csv files. The file name of the image can also be found in the .csv folder because the file name corresponds the image and .csv files. (For an instance, if the name of a .png image is "image_1.png" which is located in the rbg folder, the same name "image_1.csv" will be available in the contour folder as a .csv file. Now, the cell information of the "image.png" will be available in the file "image.csv"). As this is mentioned above that the .csv files doesn't consist of the density information of any cells, and it only consist of the cell counts. So, by dividing the tumor cell count by other cells found except tumor, density information can be obtained. Then, the images and the corresponding density information should be categorized in to 2 types such as train data and test data. As it is mentioned previously, there are 1440 images in total. so, 1000 images will be stored in the train data and 440 images will be stored in the test data. Now, the train data consists of 1000 images and its corresponding 1000 labels. similarly, the test data consists of the remaining 440 image and its corresponding labels. The image and label in the train data and test data should not same. If it's same, then the model may overfit (Tensorflow core, 2019).

3.2. Prepare Data in batches:

This is a state-of-art standard method for data pre-processing and data augmentation (Afshine., 2018), where it saves memory consumption by setting the images in batches. In this project, the batch size is set to 8, where the 8 set of images will be processed at once. This will make the processing faster and smoother. This set of batches will be used in an order for augmenting the data, processing the data and so on.

3.3. Data Augmentation:

The Deep Convolutional Neural Network requires numerous amounts of data. So, it's essential to augment the image to enhance the accuracy of tumour density prediction. The Data augmentation (TensorFlow core, 2019) can be achieved with the keras API which offers significant and different functions such as Random Rotation, Random Flip, Random Translation, and Random Contrast to make the image vary and to give more information to the model to learn.

3.4. Data pre-processing:

Uniform aspect ratio: The first thing is to make sure that all of the images in the dataset are the same size and aspect ratio. The majority of Deep Neural Net models assume a square-shaped input image, which means that each image must be evaluated for squareness and cropped accordingly.

Image Scaling: The Resnet models only accepts the image shape of (224, 224). There are many different approaches for up-scaling and down-scaling, and a library function can be used to achieve it.

3.5. Building the model:

The training of this model will take place using transfer learning techniques. The training procedure accepts any actual value as input and produces values between 0 and 1. The closer the input value is to 1.0, the closer the output value is to 0.0 (Jason, 2019). Furthermore, different pretrained models' architecture and weights will be used by removing the top layer of that model. Additionally, Global Average Pooling, Batch Normalization and dropout layers will be added before the final dense layer. Furthermore, this problem is based on regression, so Adam optimizer will be used with the Mean Squared Error loss function. Finally, the model will be trained for different epoch sizes like 25, 35 or 100. Additionally, every pre-trained model will be trained by excluding some layers. For an instance, the Resnet50 have been trained by excluding the 1st 3 layers of the model. As it is mentioned previously in the introduction that, each layer will learn different features. So, by focusing on the selective feature, accuracy of the prediction can be increased.

3.6. Testing the model:

The model which has been trained will be used to evaluate and predict the density of tumour for the new image where the tumour density of those images will be unknown. However, the evaluation will take place using the labelled data which are not used in training set. Hence, the number of correct predictions and wrong predictions will be compared to conclude the accuracy of the model. The primary focus of this model is to predict the tumour density with the least validation loss as possible.

Chapter 4: Development

4.1. Experiment 1: Resnet 50 with all layers trainable

Design:

The model construction of the 1st model carried out with Resnet 50 with all layers as trainable where it takes the input shape as (224,224,3) and the ImageNet weights has been used. Then a sequential layer has been added with this pretrained model with a final layer as Dense and activation as sigmoid. The logistic function, often known as the sigmoid activation function, has long been a popular activation function for neural networks. The function's input is converted to a value between 0.0 and 1.0 (Jason, 2019).

Implementation:

Adam is a replacement optimization algorithm for stochastic gradient descent for training deep learning models (Jason, 2017). The learning rate is a tuning parameter in an optimization algorithm that sets the step size through each iteration as it moves toward the

loss function's minimum (Jason 2019). The model is compiled with the Adam optimizer with the learning rate 0.001 and the loss function used is mean squared error with the metrics mean absolute error and mean percentage error. Then the entire model has been trained with the train data and the test data for 25 epochs. Moreover, the training history will be saved in the variable called history. This will be used for visualization of the model performance. The visualization will take place with the help of the python library matplotlib. Matplotlib is a plotting library for the Python programming language and its numerical mathematics extension NumPy. It provides an object-oriented API for embedding plots into applications using general-purpose GUI toolkits. Additionally, CSV Logger and a Model Checkpoint has been implemented. The CSV Logger will save the entire training process and will save it in the working directory as a text file where the Model Checkpoint will save the best model by comparing the validation loss in each epoch.

Testing:

The validation loss of the 1st Resnet 50 model started with 0.30 in epoch 1 and ended in 0.17 in the 25th epoch. However, the model climbed the least validation loss of 0.14 in the 24th epoch. Still, the graph (Figure: 4.1 & 4.2) clearly represents that the validation loss and mean absolute error is fluctuating. Fluctuation is the sign of model overfitting. So, the research will move further in the sense of decreasing the loss without model overfitting.

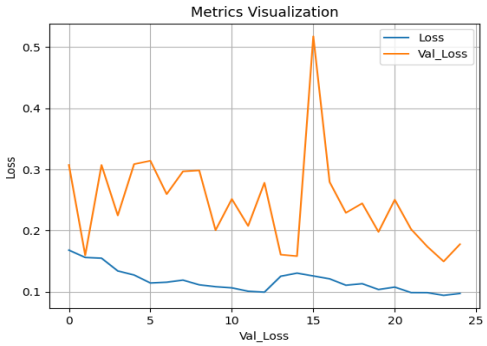

Figure 4.1: loss and validation loss

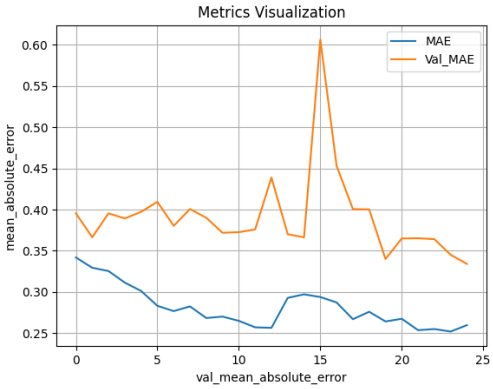

Figure 4.2: MAE and validation MAE

4.2. Experiment 2: Resnet 50 with 5th layer only trainable

Design:

The construction of the 2nd model carried out with Resnet 50 but this time only the 5th layer is trainable except the 5th layer all other layers from 0 to 4 are non-trainable where this also takes the input shape as (224,224,3) and the ImageNet weights has been used. Then a sequential layer has been added with this pretrained model with a final layer as Dense and activation as sigmoid.

Implementation:

Like the previous experiment, the model is compiled with the Adam optimizer with the learning rate 0.001 and the loss function used is mean squared error with the metrics mean absolute error and mean percentage error. Then the entire model has been trained with the train data and the test data for 25 epochs. Additionally, CSV Logger and a Model Checkpoint has been implemented in this model as well.

Testing:

The validation loss of the 2nd Resnet 50 model started with 0.25 in epoch 1 and ended in 0.19 in the 25th epoch. However, the model climbed the least validation loss of 0.19 in the 25th epoch. Still, the graph (Figure: 4.3 & 4.4) clearly represents that the validation loss and mean absolute error is fluctuating. Fluctuation is the sign of model overfitting. As I

mentioned previously, this research will move further in the sense of decreasing the loss without model overfitting. However, by looking in terms of model learning, this model performs slight better than the 1st one.

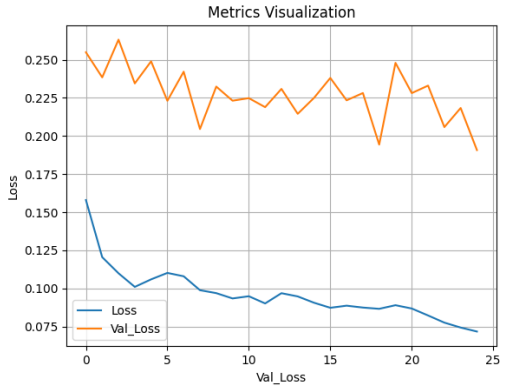

Figure 2.3: loss and validation loss

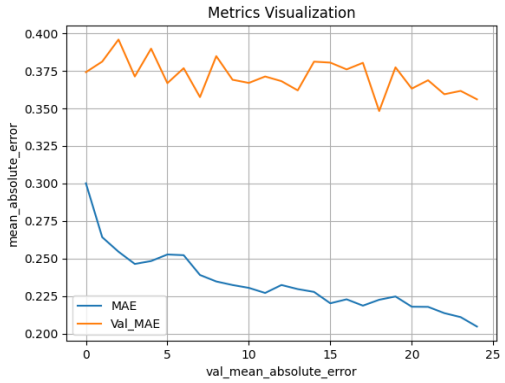

Figure 4.4: MAE and validation MAE

Comparison of Experiment 1 & Experiment 2:

The values compared below takes place with the best result obtained in every model training. As per the comparison table, the training loss of the 1st experiment is higher than the 2nd experiment. However, while comparing with the validation loss the 1st model is lower than the 2nd model. validation loss is much more important than the training loss because by selecting the best model with validation result, the prediction rate raises higher. The main objective of the project is to build a model with higher accuracy. By this comparison, it is well known that the model 1 is better than model 2. So, in next experiment comparison, model 1 will be compared with that experiment.

Experiments	Loss	Validation loss	MAE	Validation MAE
1st	0.09	0.14	0.25	0.34
2nd	0.07	0.19	0.20	0.35

Table 4-1: model 1 & 2 Comparison Table.

4.3. Experiment 3: Resnet 50 with 4 and 5th layer only trainable

Design:

The 3rd model was built with Resnet 50, however this time only the 4th and 5th layers are trainable for focusing on selective feature. All other layers from 0 to 3 are non-trainable, and the input shape is (224,224,3). ImageNet weights were utilized. Then, with this pretrained model, a sequential layer was added, with a final layer of Dense and sigmoid activation.

Implementation:

The model is developed using the Adam optimizer with a learning rate of 0.001 and a loss function of mean squared error with the metrics mean absolute error and mean percentage error, much like the previous model. The complete model was then trained for 25 epochs using the train and test data. In addition, a CSV Logger and a Model Checkpoint are added.

Testing:

The validation loss of the 3rd Resnet 50 model started with 0.28 in epoch 1 and ended in 0.19 in the 25th epoch. However, the model climbed the least validation loss of 0.19 in the 25th epoch. Still, the graph (Figure: 4.5 & 4.6) clearly represents that the validation loss and mean absolute error is fluctuating.

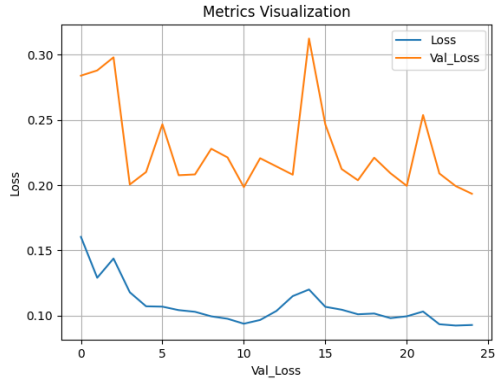

Figure 4.5: loss and validation loss

Figure 4.6: MAE and validation MAE

Comparison of experiment 1 & experiment 3:

As mentioned in the last comparison, the values compared below takes place with the best result obtained. As per the comparison table, the training loss of the 1st experiment is same as the 2nd experiment. However, while comparing with the validation loss, the 1st model is lower than the 3rd model. As it is explained previously, validation loss is much more important than the training loss because by selecting the best model with validation result, the prediction accuracy raises higher. By this comparison, it is well known that the model 1 is better than model 3.

Experiments	Loss	Validation loss	MAE	Validation MAE
1st	0.09	0.14	0.25	0.34
3rd	0.09	0.19	0.24	0.35

Table 4-2: model 1 & 3 Comparison Table.

4.4. Experiment 4: Resnet 101 with all layers trainable

Design:

The pretrained model has been altered this time where the Resnet 101 is used, and all the layers are trainable as in the first experiment, where this model also takes the input form of (224,224,3) and ImageNet weights have been utilized. Then, with this pretrained model, a sequential layer was added, with a final layer of Dense and sigmoid activation.

Implementation:

The optimizer, loss function, learning rate, and metrics remain unchanged from the previous experiment. With CSV Logger and a Model Checkpoint, the complete model was trained for 25 epochs with the train and test data.

Testing: The first Resnet 101 model's validation loss began at 0.51 in epoch 1 and terminated at 0.17 in the 25th epoch. In the 10th epoch, however, the model achieved the lowest validation loss of 0.15. Nonetheless, the graph (Figures 4.7 and 4.8) shows that the validation loss and mean absolute error are both fluctuating a bit, but the model keeps learning effectively because the validation loss keeps decreasing gradually.

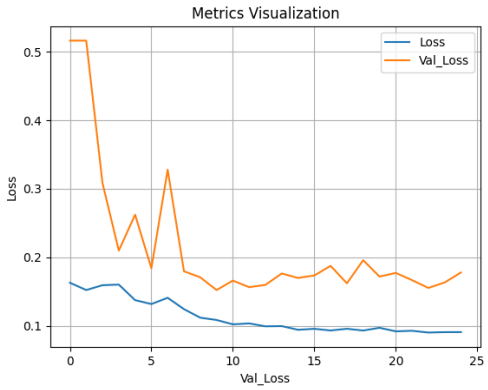

Figure 4.7: loss and validation loss

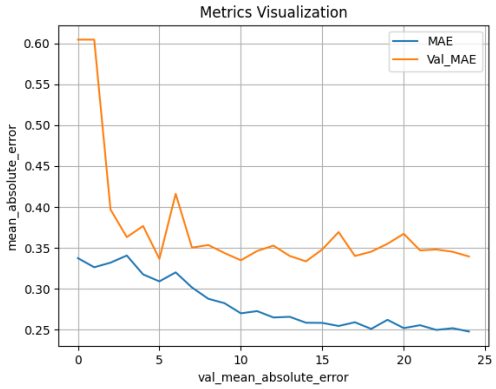

Figure 4.8: MAE and validation MAE

Comparison of experiment 1 & experiment 4:

According to the comparison table, the 1st model's training and validation losses are smaller than the 4th model's loss. It is commonly known that model 1 is superior to model 4 in terms of loss but the loss of 1st model is not decreasing like the 4th model which is the actual sign of higher overfitting. As a result, model 4 will be compared to the new model in the next model comparison.

Experiments	Loss	Validation loss	MAE	Validation MAE
1st	0.09	0.14	0.25	0.34
4th	0.10	0.15	0.28	0.34

Table 4-3: model 1 & 4 Comparison Table.

4.5. Experiment 5: Resnet 101 with 5th layer only trainable

Design:

The 5th model was developed with Resnet 101, however this time only the 5th layer is trainable; all other layers from 0 to 4 are non-trainable. The input shape is (224,224,3), and ImageNet weights were utilized. Then, with this pretrained model, a sequential layer was added, with a final layer of Dense and sigmoid activation.

Implementation:

As same as the previous model, the optimizer, loss function, learning rate, metrics are not changed. The entire model has been trained with the train data and the test data for 25 epochs with CSV Logger and a Model Checkpoint.

Testing:

The validation loss of the second Resnet 101 model began at 0.30 in epoch 1 and stopped at 0.26 in epoch 25. However, in the third epoch, the model achieved the lowest validation loss of 0.15. Nonetheless, the graph (Figures 4.9 and 4.10) shows that the validation loss and mean absolute error are fluctuating significantly.

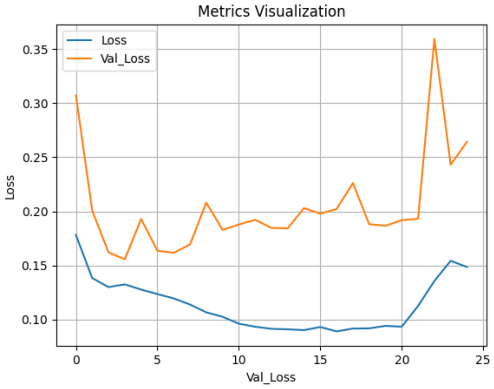

Figure 4.9: loss and validation loss

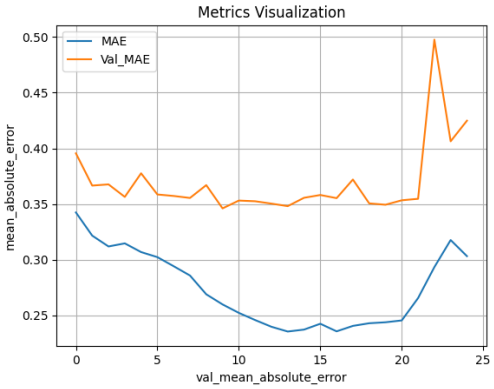

Figure 4.10: MAE and validation MAE

Comparison of experiment 4 & experiment 5:

As per the comparison table, the training loss and the validation loss of the 4th model is lower than the 5th model and the validation loss plot of the 4th model decreases better than 5th model. By this comparison, it is known that the model 4 is better than model 5. So, in next model comparison, model 4 will be compared with that new model.

Experiments	Loss	Validation loss	MAE	Validation MAE
4th	0.10	0.15	0.28	0.34
5th	0.13	0.15	0.31	0.35

Table 4-4: model 1 & 5 Comparison Table.

4.6. Experiment 6: Resnet 101 with 4 and 5th layers trainable

Design:

The model construction of the 6th model carried out with Resnet 101, but this time the 4th and 5th layer is trainable except the 4th and 5th layer all other layers from 0 to 3rd layer are non-trainable where this also takes the input shape as (224,224,3) and the ImageNet weights has been used. Then a sequential layer has been added with this pretrained model with a final layer as Dense and activation as sigmoid

Implementation:

As same as the 5th model, the optimizer, loss function, learning rate, metrics are not changed except the layers. The entire model has been trained with the train data and the test data for 25 epochs with CSV Logger and a Model Checkpoint.

Testing:

The validation loss of the 3rd Resnet 101 model started with 0.32 in epoch 1 and ended in 0.17 in the 25th epoch. However, the model climbed the least validation loss of 0.16 in the 23rd epoch. Still, the graph (Figure: 4.11 & 4.12) clearly represents that the validation loss and validation mean absolute error is fluctuating.

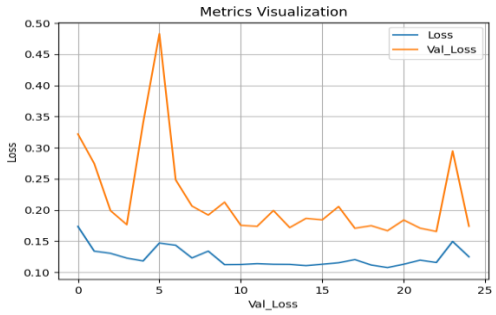

Figure 4.11: loss and validation loss

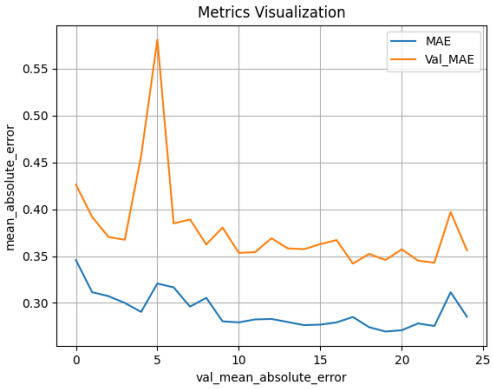

Figure 4.12: MAE and validation MAE

Comparison of experiment 4 & experiment 6:

As per the comparison table, the training loss and the validation loss of the 4th model is lower than the 6th model. By this comparison, it is known that the model 1 is better than model 6. So, in next model comparison, model 4 will be compared with that model.

Experiments	Loss	Validation loss	MAE	Validation MAE
4th	0.10	0.15	0.28	0.34
6th	0.11	0.16	0.27	0.34

Table 4-5: model 1 & 6 Comparison Table.

4.7. Experiment 7: Resnet 152 with all layers trainable

Design:

The model construction of the 7th model carried out with Resnet 152, the pretrained model has been changed in this model and all the layers are trainable as like as 4th model where this model also takes the input shape as (224,224,3) and the ImageNet weights has been used. Then a sequential layer has been added with this pretrained model with a final layer as Dense and activation as sigmoid.

Implementation:

Except the pre-trained model, the optimizer, loss function, learning rate, and metrics remain unchanged from the previous model. With CSV Logger and a Model Checkpoint, the

complete model was trained for 25 epochs with the train and test data.

Testing:

The validation loss of the 1st Resnet 152 model started with 0.30 in epoch 1 and ended in 0.15 in the 25th epoch. However, the model climbed the least validation loss of 0.15 in the 11th epoch. Still, the graph (Figure: 4.13 & 4.14) clearly represents that the validation loss and mean absolute error is fluctuating.

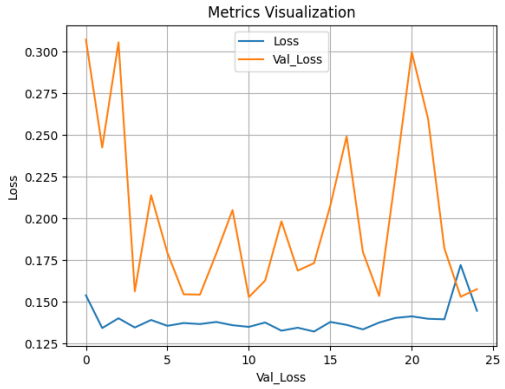

Figure 3: loss and validation loss

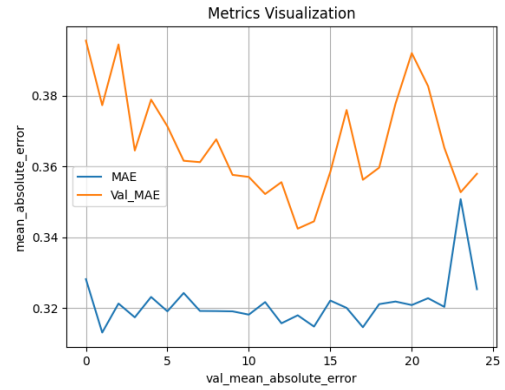

Figure 4.14: MAE and validation MAE

Comparison of Experiment 4 & Experiment 7:

According to the comparison table, the 4th model's training and validation losses are smaller than the 7th model's loss. It is clear from this comparison that model 4 is superior to model 7. As a result, model 4 will be compared to that model in the next experiment comparison.

Experiments	Loss	Validation	MAE	Validation
		loss		MAE
4th	0.10	0.15	0.28	0.34
7th	0.13	0.15	0.31	0.35

Table 4-6: model 1 & 7 Comparison Table.

4.8. Experiment 8: Resnet 152 with only 5th layer trainable

Design:

The model for the 8th model was produced with Resnet 152, however only the 5th layer is trainable this time; all other layers from 0 to 4 are non-trainable, and the input shape is (224,224,3). ImageNet weights were applied. Then, with this pretrained model, a sequential layer was added, with a final layer of Dense with sigmoid activation.

Implementation:

Except the trainable layers, the optimizer, loss function, learning rate, and metrics remain unchanged from the previous experiment. With CSV Logger and a Model Checkpoint, the complete model was trained for 25 epochs with the train and test data.

Testing:

The validation loss of the 2nd Resnet 152 model started with 0.30 in epoch 1 and ended in 0.22 in the 25th epoch. However, the model climbed the least validation loss of 0.15 in the 11th epoch. Still, the graph (Figure: 4.15 & 4.16) clearly represents that the validation loss and validation mean absolute error is fluctuating.

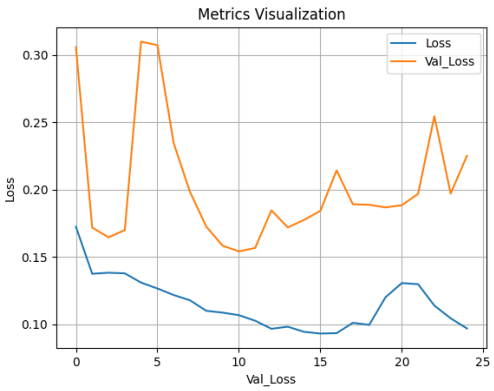

Figure 4.15: loss and validation loss

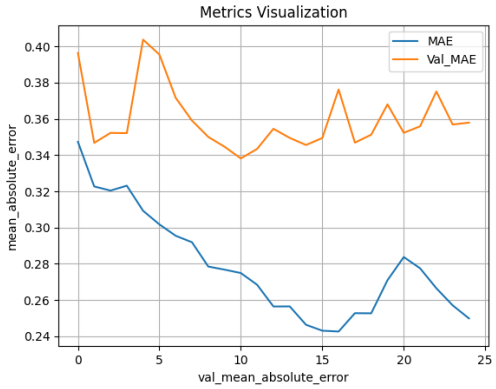

Figure 4.16: MAE and validation MAE

Comparison of Experiment 4 & Experiment 8:

As per the comparison table, the training loss and the validation loss of the 4th model is same as the 8th model. By comparing Figure (4.5 and 4.6) with the Figure (4.17 and 4.18), the model 8 performs really well than any other models which ever trained before. So, in next model comparison, model 8 will be compared with that experiment.

Experiments	Loss	Validation loss	MAE	Validation MAE
4th	0.10	0.15	0.28	0.34
8th	0.10	0.15	0.27	0.33

Table 4-7: Experiment 4 & 8 Comparison Table.

4.9. Experiment 9: Resnet 152 with 4 and 5th layer trainable

Design:

The model construction of the 9th model carried out with Resnet 152, but this time the 4th and 5th layer is trainable except the 4th and 5th layer all other layers from 0 to 3rd layer are non-trainable where this also takes the input shape as (224,224,3) and the ImageNet weights has been used. Then a sequential layer has been added with this pretrained model with a final layer as Dense and activation as sigmoid

Implementation:

As same as the 8th model, the optimizer, loss function, learning rate, metrics are not changed. The entire model has been trained with the train data and the test data for 25 epochs with CSV Logger and a Model Checkpoint.

Testing:

The validation loss of the 3rd Resnet 152 model started with 0.48 in epoch 1 and ended in 0.15 in the 25th epoch. However, the model climbed the least validation loss of 0.15 in the 25th epoch. Still, the graph (Figure: 4.17 & 4.18) clearly represents that the validation loss and validation mean absolute error is fluctuating.

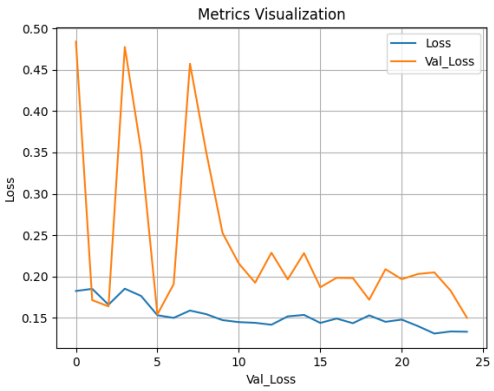

Figure 4.17: loss and validation loss

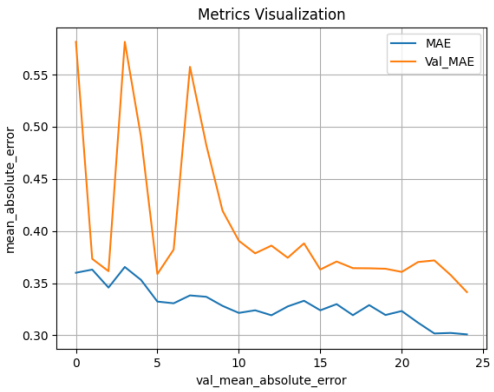

Figure 4.18: MAE and validation MAE

Comparison of model 8 & model 9:

According to the comparison table, the 8th model's training and validation losses are smaller than the 9th model's loss. It is clear from this comparison that model 8 is preferable than model 9. As a result, the 9th model created performs well, especially in

terms of validation loss. However, as previously indicated, even the Resnet 152 model with 5th layer trainable (model 8) is overfitting slightly. It is a brilliant idea to apply multiple learning rates into the model and compare outcomes to reduce model overfitting.

Experiments	Loss	Validation loss	MAE	Validation MAE
8th	0.10	0.15	0.27	0.33
9th	0.13	0.15	0.30	0.34

Table 4-8: model 8 & 9 Comparison Table.

Chapter 5: Hyperparameter optimization

5.1. Learning rate search:

The design of the model remains same as the model which we have used in model 8. However, the idea is to test different learning rates in the model Resnet 152 with all layers trainable. So, as a first step, it is planned to test learning rate from 0.01 to 1e-6. if this process is being implemented manually then it would be a time-consuming task and a human monitoring is required. So, automating this would be an excellent idea to get results soon. The Keras Tuner (Keras-team, 2019) is a python library from Keras that assists in selecting the best hyperparameters. In the tuner construction of the coding part, learning rate from 0.01 to 1e-6 is listed for training with maximum of 5 trails and 3 executions (Figure 5.1). The tuner will select the best learning rate by looking at the least validation loss as possible.

```
    resnet_model.compile(optimizer=tf.keras.optimizers.Adam(hp.Choice('learning_rate',
        values=[1e-2, 1e-3, 1e-4, 1e-5, 1e-6])),
        loss='mean_squared_error',
        metrics=["MeanAbsoluteError", "MeanAbsolutePercentageError"])
    return resnet_model

tuner = RandomSearch(
    build_model,
    objective='val_loss',
    max_trials = 5,
    executions_per_trial = 3,
    directory = 'my_dir',
    project_name = 'ResNet50_Hyperparameter_Optimization')
tuner.search_space_summary()
```

Figure 5.1: Tuner construction

After 5 hours and 6 minutes of searching, the tuner discovered the best learning rate, which is 1e-6 with a validation loss of 0.1537. However, this is nearly identical to the 0.1554 obtained in model 8. However, visualizing the tuner result is required to determine whether the model with a learning rate of 1e-6 is overfitting or not.

```
Best val_loss So Far: 0.1537813146909078
Total elapsed time: 05h 06m 40s
```

Figure 5.2: Tuner result

5.2. Increasing training size:

The epochs have been raised from 25 to 100 for testing purposes. For the Resnet model, 35 epochs are usually sufficient (Esmailian, 2019). A few other metrics, such as Mean Squared Error, Root Mean Squared Error, Mean Squared Logarithmic Error, and Cosine Similarity, have also been added (Kerasio, 2019).

After training the model for 100 epochs, the least validation loss is obtained from 26th epoch where the validation loss is 0.15. The visualization history of the whole training result has been shown below (Figure 5.3).

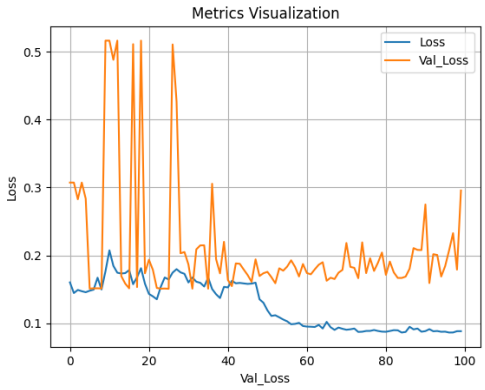

Figure 5.3: loss and validation loss

The graph (Figure 5.3) clearly shows that the model overfits even after training for 100 epochs with a learning rate of 0.005. The higher the learning rate, the higher the model overfits, according to the learning rate pattern.

From this hyperparameter optimization techniques, we get to know that the learning rate 1e-6 is the optimal learning rate for this Resnet 152 model with all layers trainable and by training the model for 100 epochs, in the

plot (Figure 5.3), the fluctuation is less between the epochs 40 and 70. So it's also a great idea to reduce model overfitting.

Chapter 6: Development Phase - 2

6.1. Resnet 152 Model Optimization:

6.1.1. 1st model: Design & Implementation

The model construction for phase 2 model 1 was done with Resnet 152 and all layers set to trainable, with the input shape being (224,224,3) with ImageNet weights. Then, with this pretrained model, a sequential layer was added, with a final layer of Dense and sigmoid activation. The model is also trained for 100 epochs at a learning rate of 1e-6. The ideal learning rate for our model is 1e-6, which was determined through hyperparameter tweaking. Furthermore, as previously noted, 7 other measures have been included for examination. From Figure, a depiction of the metrics history is presented below (6.1 to 6.5).

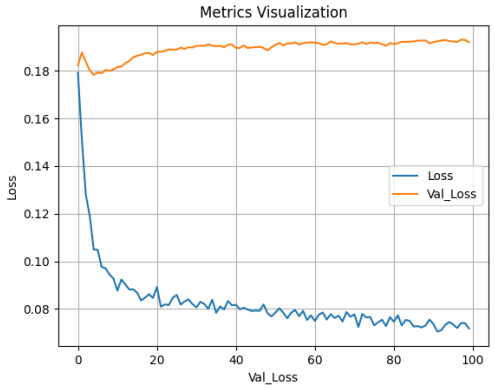

Figure 4: loss and validation loss

Testing:

The validation loss of this model Resnet 152 started with 0.18 in epoch 1 and ended in 0.19 in the 100th epoch. However, the model climbed the least validation loss of 0.18 in the 26th epoch. While comparing this model with the model which is trained on the 8th experiment, the model trained on 8th experiment has the least validation loss of 0.15 and the model trained with this optimization technique has the least validation loss of 0.18. However, model trained on phase 1, 8th experiment has the least validation loss, which is comparatively good, and the model trained in the 8th experiment overfits a bit (Figure 4.15) and here the model after optimization overfits (Figure 6.1).

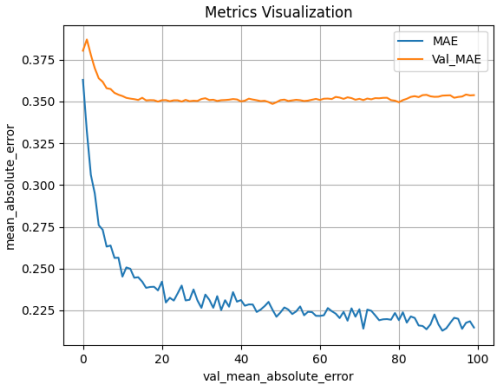

Figure 6.2: MAE and validation MAE

The train mean absolute error started with 0.36 and ended in 0.21 and the validation mean absolute error started with 0.38 and ended in 0.35 while reaching 100th epoch of this Resnet 152 model which is trained on phase 2 model 1.

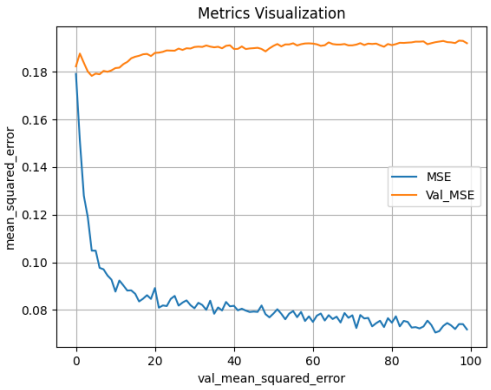

Figure 6.3: MSE and validation MSE

While reaching the 100th epoch of this Resnet 152 model, which was trained on phase 2 model 1, the train mean squared error was 0.17 and ended in 0.07, while the validation mean squared error was 0.18 and ended in 0.19.

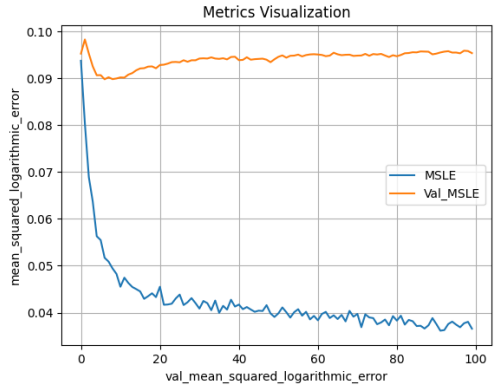

Figure 6.4: MSLE and validation MSLE

While reaching the 100th epoch of this Resnet 152 model, which was trained on phase 2 experiment 1, the train mean squared logarithmic error started with 0.09 and ended in 0.03 and the validation mean squared logarithmic error started with 0.09 and concluded in 0.09, respectively.

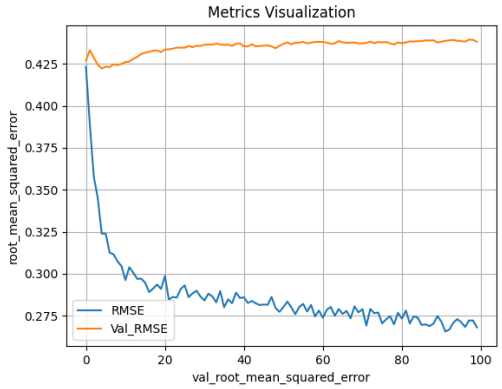

Figure 6.5: RMSE and validation RMSE

The train root mean squared error started with 0.42 and ended in 0.26 and the validation root mean squared error started with 0.42 and ended in 0.43 while reaching 100th epoch of this Resnet 50 model which is trained on phase 2 model 1.

6.1.2. 2nd Experiment: Design & Implementation

The model construction of phase – 2, model 2 carried out with Resnet 152 with all layers as trainable where it takes the input shape as (224,224,3) and the ImageNet weights has been used. Then a sequential layer has been added with this pretrained model with a final layer as Dense and activation as sigmoid. Additionally, a dropout layer with a ratio of 0.2 has been added to the deep neural network. Here the overall design of the model remains same as the phase 2, 1st model except, the dropout layer which is newly added to this model. Furthermore, the model is trained for 100 epochs with the learning rate 1e-6. The learning rate 1e-6 is the optimal learning rate for our model which is obtained by hyperparameter optimization. The visualization of the metrics history has been shown below from Figure (6.6 – 6.10).

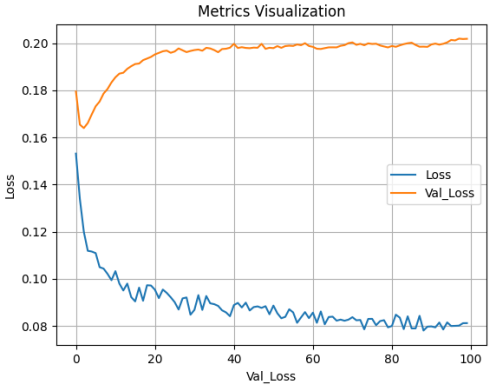

Figure 6.6: loss and validation loss

Testing:

This model Resnet 152's validation loss began at 0.17 in epoch 1 and concluded at 0.20 in the 100th epoch. However, in the third epoch, the model achieved the lowest validation loss of 0.16. When compared to a model trained on phase 2, 1st model, the model trained on phase 2, 2nd experiment has the lowest validation loss of 0.16, while the model trained on phase 2, 1st model has the highest validation loss of 0.18. However, the graphs (Figure 6.6) show that the model is overfitting, and validation loss fell from 0.18 to 0.16 after

adding the dropout layer to model.

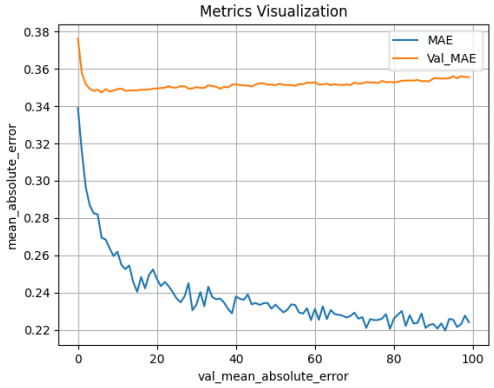

Figure 6.7: MAE and validation MAE

The train mean absolute error started with 0.33 and ended in 0.24 and the validation mean absolute error started with 0.37 and ended in 0.35 while reaching 100th epoch of this Resnet 152 model which is trained on phase 2 model 2.

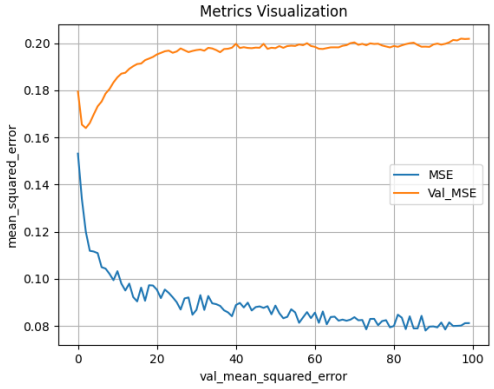

Figure 6.8: MSE and validation MSE

The train mean squared error started with 0.15 and ended in 0.08 and the validation mean squared error started with 0.17 and ended in 0.20 while reaching 100th epoch of this Resnet 152 model which is trained on phase 2 model 2.

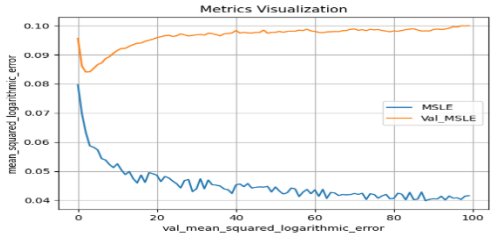

Figure 6.9: MSLE and validation MSLE

While reaching the 100th epoch of this Resnet 152 model, which was trained on phase 2 model 2, the train mean squared logarithmic error started at 0.04 and concluded at 0.07, and the validation mean squared logarithmic error started at 0.09 and ended in 0.09, respectively.

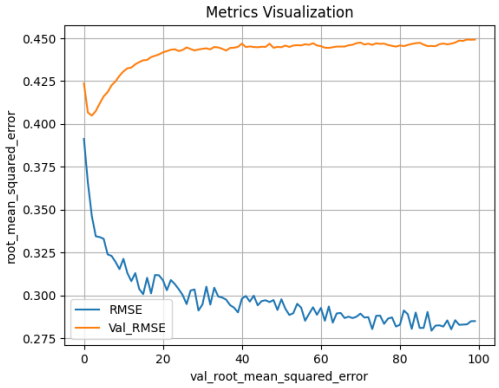

Figure 5: RMSE and validation RMSE

The train root mean squared error started with 0.39 and ended in 0.28 and the validation root mean squared error started with 0.42 and ended in 0.44 while reaching 100th epoch of this Resnet 50 model which is trained on phase 2 model 2.

6.1.3. 3rd model: Design & Implementation

The model construction of phase – 2, model 3 carried out with Resnet 152 with all layers as trainable where it takes the input shape as (224,224,3) and the ImageNet weights has been used. Then a sequential layer has been added with this pretrained model with a final layer as Dense and activation as sigmoid as same as the previous model trained. Additionally, a dropout layer with a ratio of 0.5 has been added to the deep neural network. Here the overall design of the model remains same as the phase 2, 2nd model except, the ratio of dropout layer is increased to the model. Furthermore, the model is trained for 100 epochs with the learning rate 1e-6. The visualization of the metrics history has been shown below from Figure (6.11 to 6.15).

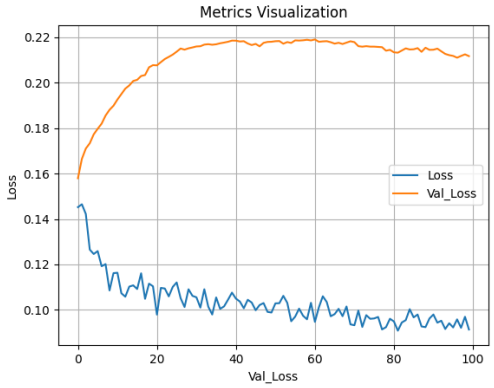

Figure 6: loss and validation loss

Testing:

The validation loss of this model Resnet 152 started with 0.15 in epoch 1 and ended in 0.21 in the 100th epoch. However, the model climbed the least validation loss of 0.15 in the 1st epoch after the 1st epoch there is no reduction in validation loss, the loss is kept on increasing slowly. While comparing this model with the model which is trained on the phase 2, 2nd model, the model trained on phase 2, 3rd model has the least validation loss of 0.15 and the model trained on phase 2, 2nd model has the validation loss of 0.16. However, the plot (Figure 6.11) clearly states that the model is overfitting, but the model 3rd is not learning, it started increasing the validation loss and the least loss obtained is from the epoch 1.

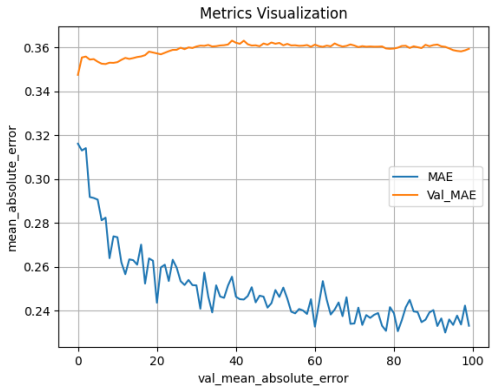

Figure 6.12: MAE and validation MAE

While reaching the 100th epoch of this Resnet 152 model, which was trained on phase 2, 3rd model, the train mean absolute error started at 0.31 and concluded at 0.23, while the validation mean absolute error started at 0.34 and ended at 0.35.

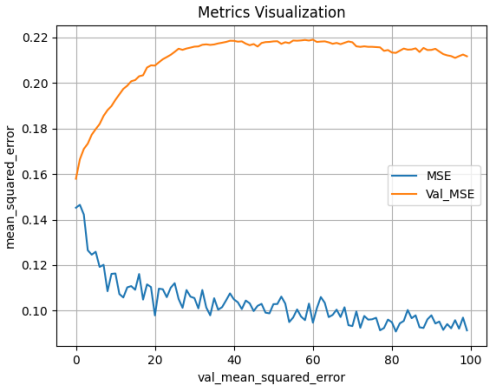

Figure 6.137: MSE and validation MSE

The train mean squared error started with 0.14 and ended in 0.09 and the validation mean squared error started with 0.15 and ended in 0.21 while reaching 100th epoch of this Resnet 152 model which is trained on phase 2 model 3.

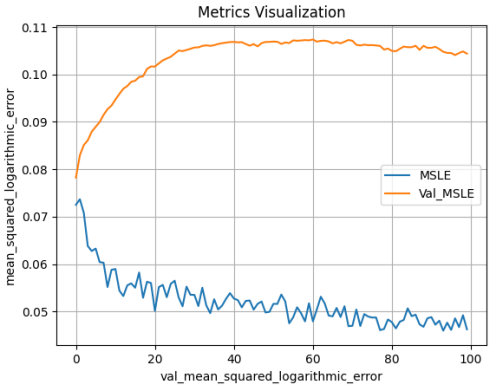

Figure 6.14: MSLE and validation MSLE

The train mean squared logarithmic error started with 0.07 and ended in 0.04 and the validation mean squared logarithmic error started with 0.07 and ended in 0.10 while reaching 100th epoch of this Resnet 152 model which is trained on phase 2 model 3.

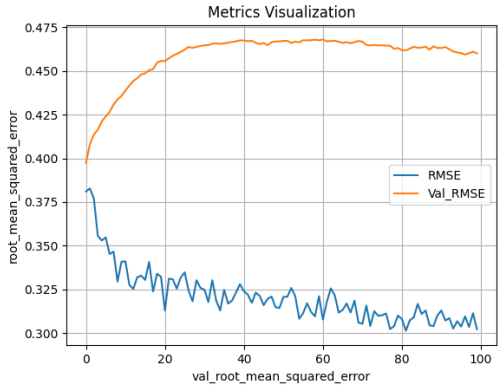

Figure 6.158: RMSE and validation RMSE

While reaching the 100th epoch of this Resnet 152 model, which was trained on phase 2 model 3, the train root mean squared error started at 0.38 and concluded at 0.30, and the validation root mean squared error started at 0.39 and ended at 0.46.

Chapter 7: Conclusion

7.1. Summary of the project:

To conclude, this research achieved all the objectives that are specified. As a first step, density has been calculated with the use of cell groups and used it along with the histopathological image data and transmitted to the standard data generator class for pre-processing and data augmentation. As it is mentioned previously, data augmentation took place with random rotation, random flip, random contrast and so on. These pre-processed inputs have been successfully trained and the results were obtained. In top of that, there are totally, 12 models have been trained, validated, and compared. As per the result, the models which ever trained before hyperparameter optimization are slightly overfitting and the Resnet 152 model which is trained on the phase 1, 8th experiment has the good validation accuracy of 0.15 which is 15% approximately and the overfitting of this model is less compared to other trained models.

On the other hand, the models which ever trained after performing hyperparameter optimization, are highly overfitting and totally 3 models have been trained which is the part of 12 models as it is mentioned above. These last 3 model development is considered as a phase 2. In phase 2, the 2nd experiment carried out has the low validation loss but it's not as good as the phase 1, 8th model because it is overfitting highly.

As a result, the model trained on phase 1, experiment 8 outperforms than others, and it is a good choice for predicting tumor cell density.

7.2. Future work:

This exploration can be improved in the future by using these data to train more complicated models and performing more difficult hyperparameter optimization approaches like as regularization, K-fold Cross validation, Feature selection, integrating other datasets, or augmenting more photos. Following that, software for estimating density in real-time webcam feeds can be developed. It is possible to normalize the frames. The model can be used to forecast tumor density using acquired normalized frames. However, this is a highly advanced technology that necessitates a wide range of needs, compatibility, and constraints (OHS, 2018).

References:

AFSHINE, A., SHERVINE, A. 2018. Keras Data Generator: *A detailed example of how to use data generators with Keras.* [Blog online]. 3 April. Available from: https://stanford.edu/~shervine/blog/keras-how-to-generate-data-on-the-fly# [Accessed 3 February 2022].

MOHAMED, A. 2021. Computer Vision and Pattern Recognition: *NuCLS: A scalable crowdsourcing, deep learning approach and dataset for nucleus classification, localization, and segmentation.* [online]. 2102, pp. 1-45. Available from: https://arxiv.org/ftp/arxiv/papers/2102/2102.09099.pdf [Accessed 24 January 2022].

NADIA, B., GIUSEPPE, P., MARIA, F., DANIEL, R., 2019. A Deep Learning Approach for Breast Invasive Ductal Carcinoma Detection and Lymphoma Multi-Classification in Histological Images. *In: 2020 IEEE International Conference on Industrial Technology (ICIT),* 28 March 2019, pp. 1 – 12.

JASON, B. 2019. *A Gentle Introduction to the Rectified Linear Unit (ReLU)* [online]. Available from: https://machinelearningmastery.com/rectified-linear-activation-function-for-deep-learning-neural-networks/ [Accessed 13th March 2022].

JASON, B. 2017. *Gentle Introduction to the Adam Optimization Algorithm for Deep Learning* [online]. Available from: https://machinelearningmastery.com/adam-optimization-algorithm-for-deep-learning/ [Accessed 17th March 2022].

JASON, B. 2019. *Understand the Impact of Learning Rate on Neural Network Performance* [online]. Available from: https://machinelearningmastery.com/understand-the-dynamics-of-learning-rate-on-deep-learning-neural-networks/ [Accessed 18th March 2022].

LESHEM, E., 2018. IBM Watson Health AI gets access to full health data of 61m Italians. [Blog Online] 18 January. Available From: https://medium.com/@qData/ibm-watson-health-ai-gets-access-to-full-health-data-of-61m-italians-73f85d90f9c0 [Accessed 1st March 2022].

KAIMING, H., XIANGYU, Z., SHAOQING, R., JIAN, S. 2015. Computer Vision and Pattern Recognition. *Deep Residual Learning for Image Recognition* [online]. 1512, pp. 1-12. Available from: https://arxiv.org/pdf/1512.03385.pdf [Accessed 6 February 2022].

ERIN, J., AIELLO, 1., DIANA, S., BUIST, M., EMILY, W., PEGGY, P. 2005. Association between mammographic breast density and breast cancer tumour characteristics. *Cancer Epidemiol Biomarkers Prev* [online]. 14 (3), pp. 1

Pierce, J., Natarajan, L., Caan, B., Parker, B., Greenberg, E., Flatt, S., Rock, L., Kealey, S., Al-Delaimy W., Bardwell, W. 2007. et al. Influence of a diet very high in vegetables, fruit, and fiber and low in fat on prognosis following treatment for breast cancer: *The Women's Healthy Eating and Living (WHEL) randomized trial.* JAMA [online]. *506 (3), pp. 5-19.*

WEIND, K., MAIER, C., RUTT, B., MOUSSA, M. 1998. Invasive carcinomas and fibroadenomas of the breast. comparison of micro vessel distributions--implications for imaging modalities. *Radiology* [online]. 208 (2), pp. 1.

NARESH, K., NIDHI, M. 2018. Breast Cancer Detection from Histopathological Images Using Deep Learning. In: *2018 3rd International Conference and Workshops on Recent Advances and Innovations in Engineering (ICRAIE)*, 22-25 November 2018, India [online]. Institute of Electrical and Electronics Engineers. pp. 1-4

Ritu, L. 2014. A Brief History of Breast Cancer. *Surgical domination reinvented* [online]. 14 (2), pp. 2-4. Available from: https://www.ncbi.nlm.nih.gov/pmc/articles/PMC3997531/ [Accessed 4 February 2022].

CASEY, L. 2020. Deep Learning. *Project Final Report* [online]. 128, pp. 4-8. Available from: http://cs230.stanford.edu/projects_spring_2020/reports/38922168.pdf [Accessed 6 February 2022].

FENECH, M., STRUKELJ, N. and BUSTON, O. 2018. Ethical, social, and political challenges of artificial intelligence in health. United Kingdom. Future advocacy Welcome Trust, 27 February 2018, pp. 24 – 46. Available from: https://wellcome.org/sites/default/files/ai-in-health-ethical-social-political-challenges.pdf [Accessed 1st March 2022].

METIN, N., GURCAN, P., LAURA, B., ALI, CAN., ANANT, M., NASIR, R., AND BULENT, YENER. 2010. Histopathological Image Analysis. *A Review* in *IEEE Reviews in Biomedical Engineering* [Online]. (2), pp. 147-171.

BARTELS, P., THOMPSON, D., BIBBO, M., WEBER, J. 1992. Bayesian belief networks in quantitative histopathology. *Anal Quant Cytol Histol* [online]. 14 (6), pp. 3-5. Available from: https://europepmc.org/article/med/1292445 [Accessed 3 February 2022].

HAMILTON, P., ANDERSON, N., BARTELS, P., THOMPSON, D. 1994. Expert system support using Bayesian belief networks in the diagnosis of fine needle aspiration biopsy specimens of the breast. *J Clin Pathol.* 47 (4), pp. 8-16. Available from: https://jcp.bmj.com/content/47/4/329.abstract [Accessed 2 February 2022].

RUBIN, R., STRAYER, D., RUBIN, E., MCDONALD, J. 2012. RUBIN'S PATHOLOGY: Clinicopathology Foundations of Medicine. 5th ed. London: Lippincott Williams & Wilkins. pp. 10 – 16.

MINGXING, T., QUOC, L., 2019. Machine Learning: *Efficient Net: Rethinking Model Scaling for Convolutional Neural Networks.* [online]. 1905, pp. 1-11. Available from: https://arxiv.org/pdf/1905.11946.pdf [Accessed 28 January 2022].

LUSINE, Y., GRAHAM, A., LAURA, C., STUART, J., BERNARD, R., CELINE, V., RULLA, M. 2011. Mammographic breast density and subsequent risk of breast cancer in postmenopausal women according to tumour characteristics. J Natl Cancer Inst [online]. 103 (15), pp. 2.

NUMFOCUS, 2008. *pandas* [online]. Available from: https://pandas.pydata.org/ [Accessed from 3rd March 2022].

TENSORFLOW CORE, 2019. *Overfit and underfit* [online]. Available from: https://www.tensorflow.org/tutorials/keras/overfit_and_underfit [Accessed 15th March 2022].

TENSORFLOW CORE, 2019. *Data augmentation* [online]. Available from: https://www.tensorflow.org/tutorials/images/data_augmentation [Accessed 15th March 2022].

Keras team, 2019. *KerasTuner* [online]. Available from: https://keras.io/keras_tuner/ [Accessed 1st April 2022].

Esmailian, 2019. *Is a large number of epochs good or bad idea in CNN?* [online]. Available from: https://datascience.stackexchange.com/questions/46523/is-a-large-number-of-epochs-good-or-bad-idea-in-cnn [Accessed 3 April 2022].

Kerasio, 2019. *Regression metrics* [online]. Available from: https://keras.io/api/metrics/regression_metrics/ [Accessed 10th April 2022].